

Afterpulsing and instability in superconducting nanowire avalanche photodetectors

F. Marsili, F. Najafi, E. Dauler, R. J. Molnar, and K. K. Berggren

Citation: *Appl. Phys. Lett.* **100**, 112601 (2012); doi: 10.1063/1.3691944

View online: <http://dx.doi.org/10.1063/1.3691944>

View Table of Contents: <http://apl.aip.org/resource/1/APPLAB/v100/i11>

Published by the [American Institute of Physics](http://www.aip.org).

Related Articles

Origin of intrinsic dark count in superconducting nanowire single-photon detectors

Appl. Phys. Lett. **99**, 161105 (2011)

Si-interdiffusion in heavily doped AlN-GaN-based quantum well intersubband photodetectors

Appl. Phys. Lett. **98**, 241101 (2011)

Spatial dependence of output pulse delay in a niobium nitride nanowire superconducting single-photon detector

Appl. Phys. Lett. **98**, 201116 (2011)

High detectivity squaraine-based near infrared photodetector with nA/cm² dark current

APL: Org. Electron. Photonics **4**, 32 (2011)

High detectivity squaraine-based near infrared photodetector with nA/cm² dark current

Appl. Phys. Lett. **98**, 073303 (2011)

Additional information on *Appl. Phys. Lett.*

Journal Homepage: <http://apl.aip.org/>

Journal Information: http://apl.aip.org/about/about_the_journal

Top downloads: http://apl.aip.org/features/most_downloaded

Information for Authors: <http://apl.aip.org/authors>

ADVERTISEMENT

NEW!

iPeerReview

AIP's Newest App



Authors...
Reviewers...

Check the status of
submitted papers remotely!

AIP | Publishing

Afterpulsing and instability in superconducting nanowire avalanche photodetectors

F. Marsili,¹ F. Najafi,¹ E. Dauler,² R. J. Molnar,² and K. K. Berggren^{1,a)}

¹Department of Electrical Engineering and Computer Science, Massachusetts Institute of Technology, 77 Massachusetts Avenue, Cambridge, Massachusetts 02139, USA

²Lincoln Laboratory, Massachusetts Institute of Technology, 244 Wood St., Lexington, Massachusetts 02420, USA

(Received 10 December 2011; accepted 12 February 2012; published online 13 March 2012)

We investigated the reset time of superconducting nanowire avalanche photodetectors (SNAPs) based on 30 nm wide nanowires. We studied the dependence of the reset time of SNAPs on the device inductance and discovered that SNAPs can provide a speed-up relative to superconducting nanowire single-photon detectors with the same area but with some limitations: (1) Reducing the series inductance of SNAPs (necessary for the avalanche formation) could result in the detectors operating in an unstable regime, (2) a trade-off exists between maximizing the bias current margin and minimizing the reset time of SNAPs, and (3) reducing the reset time of SNAPs below ~ 1 ns resulted in afterpulsing. © 2012 American Institute of Physics. [<http://dx.doi.org/10.1063/1.3691944>]

Superconducting nanowire avalanche photodetectors (SNAPs, also referred to as cascade-switching superconducting single-photon detectors¹) are based on a parallel-nanowire architecture that performs single-photon counting with signal-to-noise ratio (SNR) up to a factor of ~ 4 higher² than traditional superconducting nanowire single-photon detectors (SNSPDs).^{3,4} Although we recently worked to improve our understanding of the operation mechanism of SNAPs,^{2,5} the claim that these devices can operate at higher speed than SNSPDs (Ref. 1) has not yet been confirmed experimentally. We studied the reset time of SNAPs and found that although SNAPs can provide a speed-up relative to SNSPDs with the same area, the device speed is limited by the thermal relaxation of the nanowires.

We investigated the possibility of reducing the reset time of SNAPs below 1 ns by varying the number of sections in parallel (N) and by decreasing the device series inductance (L_S) necessary for the avalanche formation.¹ Indeed, as the equivalent kinetic inductance of N nanowires in parallel is N^2 times lower than their inductance in series, a N -parallel-section SNAP (N -SNAP) would be N^2 times faster than a SNSPD of the same active area, if one were to neglect certain non-idealities of the device. SNAPs operate by having the current from the section which switches to the normal state after absorbing a photon (initiating section) drive the still-superconducting sections (secondary sections) normal, resulting in a current redistribution to the read-out (modeled as a resistor R_{load}).^{2,5} Ideally, no current from the initiating section should be diverted to R_{load} before the secondary sections have switched to the normal state (we call this ideal operation mechanism *perfect redistribution*²). However, in practice, the current leaking to R_{load} (we call this current *leakage current*, I_{lk}) can be substantial. The series inductor is used to minimize the leakage current, and it has a dominant effect on the device speed.¹

We studied the effect of reducing L_S on the device operation by introducing a unitless parameter r , which we defined as the ratio between I_{lk} and the current redistributing to all the secondary sections after the initiating section switches to the normal state. For perfect redistribution, $r = 0$. Considering times much shorter than the reset time (so that the inductive impedance dominates the read-out resistance, which is typically $R_{\text{load}} = 50 \Omega$), $r = L_0/[L_S \cdot (N - 1)]$,⁶ where L_0 is the kinetic inductance of one section. Therefore, when decreasing L_S (and thus the detector reset time), the leakage current increases, and a higher bias current is necessary to ensure an avalanche.

We characterized $\sim 100 N$ -SNAPs with $N = 2, 3$, and 4 and with r ranging from 0.1 to 2 (Ref. 7) by measuring the photoresponse count rate and the photoresponse inter-arrival time histograms (see supplementary material¹⁸ and Ref. 2 for details of the fabrication process, detector geometry, and experimental setup). We found that, depending on r and on the bias current, devices could exhibit (1) correct operation as single-photon detectors (avalanche regime²), (2) operation in arm-trigger regime,² (3) unstable operation, or (4) afterpulsing.

An unstable operating regime of SNAPs was observed in devices with low L_S ($r > 0.1$) biased at low current, before the onset of the arm-trigger regime. In the unstable regime, after a hotspot nucleation (HSN) event (caused either by the absorption of a photon or by a dark count) occurred in one of the sections of the SNAP, the device emitted multiple current pulses. These trains of pulses resulted in a spurious peak in the normalized photoresponse count rate (PCR) vs normalized bias current (I_B/I_{SW} , where I_{SW} is the device switching current, defined as the highest I_B the device was able to sustain before switching to the normal state) curves, as shown in Figure 1(a) for a 3-SNAP. As the PCR in this operating regime was only weakly dependent on the photon flux incident on the device (increasing the photon flux by a factor of ~ 15 changed the count rate by a factor of ~ 4 (Ref. 8)), normalization by the applied photon flux (see supplementary material for details¹⁸) meant that the amplitude of the spurious

^{a)} Author to whom correspondence should be addressed. Electronic mail: berggren@mit.edu.

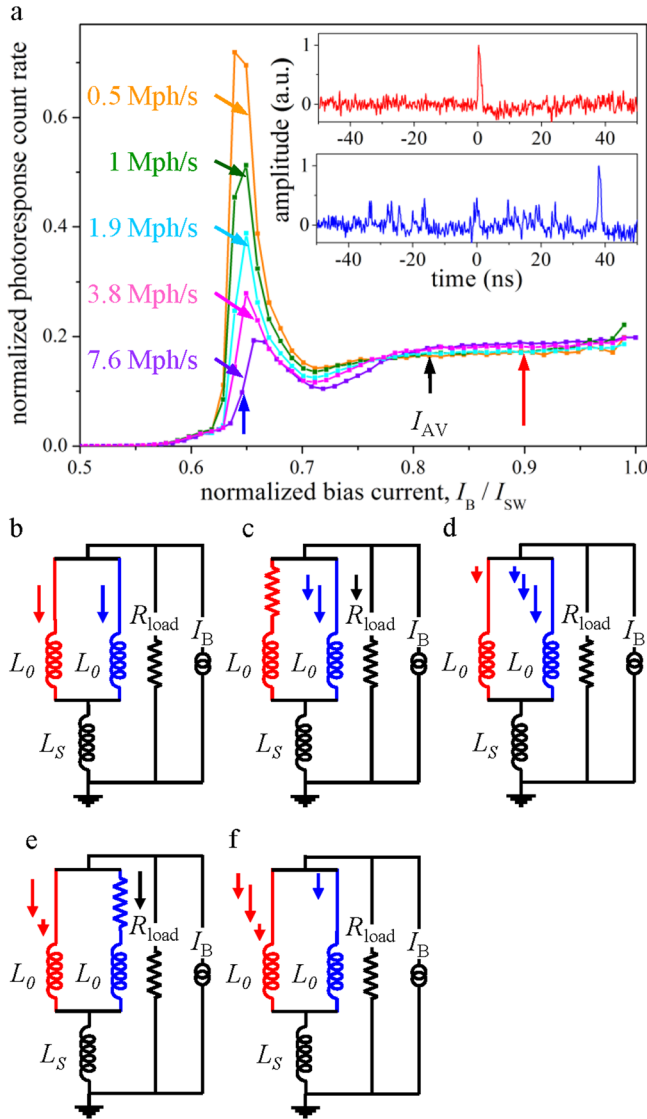


FIG. 1. (Color online) (a) Normalized PCR vs normalized I_B of a 30-nm-wide 3-SNAP ($1.47 \mu\text{m} \times 830 \text{ nm}$ active area) at different photon fluxes (expressed in photons per second: ph/s). The PCR is normalized to the photon flux (see supplementary material¹⁸). The kinetic inductance of one section was $L_0 = 13 \text{ nH}$ (estimated from the fall time of the detector response pulse), and the value of the series inductor was $L_S = 1.8 L_0$ ($r = 0.28$). The detector I_{AV} , marked by an arrow, was determined experimentally as reported in Ref. 2. Inset: Oscilloscope traces of the photoresponse of the 3-SNAP of Figure 1(a) measured in the unstable ($I_B = 0.65 I_{SW}$, lower panel) and avalanche regimes ($I_B = 0.9 I_{SW}$, upper panel). The two bias currents are marked by arrows in Figure 1(a). (b-f) Electrical equivalent circuit of the different states of a 2-SNAP operating in the unstable regime.

peak decreased with increasing optical power. The normalized PCR vs I_B curves indicated that the devices transitioned through three operating regimes as the bias current was increased: (1) the unstable regime ($0.62 \lesssim I_B/I_{SW} \lesssim 0.7$), (2) the arm-trigger regime ($0.7 \lesssim I_B/I_{SW} \lesssim 0.82$), and (3) the avalanche regime ($I_B/I_{SW} \gtrsim 0.82$). The devices worked as single-photon detectors only when operating in the avalanche regime, in which the normalized PCR could then be identified with the detection efficiency. Indeed, in the arm-trigger regime, two or more HSN events were necessary to produce a count,² and in the unstable regime, one single HSN event produced multiple counts. The inset of Figure 1(a) shows the oscilloscope traces of a detector response in

the unstable (lower panel) and the avalanche regimes (upper panel). In the unstable regime, pulses with two distinct average amplitudes were recorded (which we called “small” and “large” pulses⁹). Unlike the arm-trigger and avalanche regimes (discussed in Ref. 2), the unstable regime was not previously observed, so we will discuss it in detail here.

Figure 1(b)–1(f) illustrate our explanation for the unstable regime. Figure 1(b) shows the electrical equivalent of an unstable 2-SNAP in the steady state. After a HSN event occurs in section 1 (on the left-hand side, see Figure 1(c)), no avalanche is formed because a large part of the redistributed current leaks into R_{load} . Once section 1 switches back to the superconducting state (Figure 1(d)), the current in each of the SNAP sections increases at the same rate but from different initial conditions. Indeed, while section 1 is depleted of current, section 2 (on the right-hand side) is biased close to I_{SW} , as its current was not depleted by the initial HSN event. When the current in section 2 exceeds its I_{SW} and section 2 switches to the normal state (Figure 1(e)), the resulting current redistribution (Figure 1(f)) brings the system back to the non-stationary state (section 1 normal, section 2 superconducting) illustrated in Figure 1(c). From this point on, the different branches of the circuit continue swapping their current periodically, which causes the small pulses observed experimentally. Large pulses are then generated when an avalanche forms in the device as a result of the occurrence of several subsequent HSN events during the instability cycle. The avalanche stops the instability cycle and restores the device to the stationary condition illustrated in Figure 1(b). To support our model of the device operation, we simulated the current dynamics of a 2-SNAP and a 3-SNAP with $r = 1$ by using the electrothermal model described in Ref. 5 and reproduced the unstable regime (see supplementary material¹⁸).

We reduced the photoresponse fall time of SNAPs (the time constant of the exponential decay of the detector response pulse) by decreasing the device L_S as shown in Figure 2(a) for 4-SNAPs (for $r = 0.125$ to 1). However, the resulting decrease in fall time came at the price of an increased avalanche current (I_{AV}) as shown in Figure 2(b), where the avalanche currents of the same detectors shown in Figure 2(a) are marked by colored arrows on the normalized PCR vs bias current curves. The values of I_{AV} were determined experimentally as reported in Ref. 2. A high I_{AV} is undesirable because the bias range in which the devices operate as low-jitter single-photon detectors decreases with increasing I_{AV} (as reported in Refs. 2 and 10). Therefore, we concluded that a trade-off exists between minimizing the reset time and maximizing the bias margin of these devices.

Figure 2(c) shows the dependence of the experimental values of the avalanche current on N and r . When characterizing 2-, 3-, and 4-SNAPs with decreasing values of L_S , we observed an increase in I_{AV} with increasing r . The increase in I_{AV} was more pronounced for SNAPs with low N , because for a certain value of I_{lk} , the current redistributed to each secondary section is $I_{lk}/(N-1)$ lower than in case of perfect redistribution. The leakage current causes a larger increase in the avalanche current for lower N because the ratio between $I_{lk}/(N-1)$ and the bias current of each secondary section is larger. This behavior was predicted by an approximate model of the

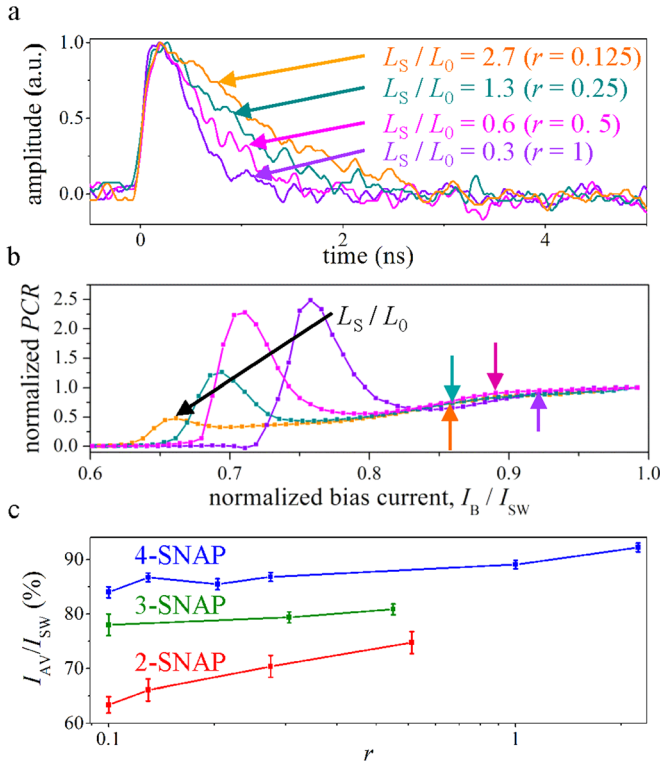


FIG. 2. (Color online) (a) Single-shot oscilloscope trace of the photoresponse pulses of 30-nm-wide 4-SNAPs ($1.47 \mu\text{m} \times 1.43 \text{ nm}$ active area) with different values of L_S . The kinetic inductance of one section was $L_0 = 13 \text{ nH}$ (estimated from the fall time of the detector response pulse). The devices were biased in avalanche regime, at $I_B = 0.98 I_{SW}$. The waveforms were normalized by their maximum. (b) PCR (normalized to the PCR at the switching current) vs I_B/I_{SW} of the same 4-SNAPs shown in Figure 2(a). The photon flux on the device active area was $2.0 \times 10^7 \text{ ph/s}$. (c) I_{AV} vs r for 2-, 3- and 4-SNAPs.

device operation which assumes that all the current of the initiating section is redistributed to the secondary sections and to R_{load} (see supplementary material¹⁸).

We performed time-resolved measurements to verify whether the decrease in the photoresponse fall time shown in Figure 2(a) corresponded to an effective decrease in the detector reset time (as the reset time and the photoresponse fall time scale differently with the device inductance in similar detectors^{11,12}). Figures 3(a) and 3(b) show the measured oscilloscope persistence traces and the photoresponse inter-arrival time histograms of the same devices shown in Figures 2(a) and 2(b), when biased in avalanche regime (at $I_B = 0.98 I_{SW}$). Strikingly, we observed that all detectors with a reset time below $\sim 1 \text{ ns}$ (estimated as in Ref. 2) showed afterpulsing, as shown in Figure 3(a). The afterpulsing also manifested itself in a peak in the inter-arrival time histograms shown in Figure 3(b). Although every sub-ns-reset-time device exhibited afterpulsing, the afterpulsing was not observed on every photoresponse pulse,¹³ as shown by the oscilloscope persistence trace.

The afterpulsing we observed on our sub-1-ns-reset-time devices is a different phenomenon from the unstable regime shown in Figure 1 and from the afterpulsing due to the read out circuit¹⁴ (see supplementary material¹⁸). We attributed the origin of the afterpulsing to the thermal relaxation dynamics of the superconducting nanowires. To support our hypothesis, we used the electrothermal model to simulate the

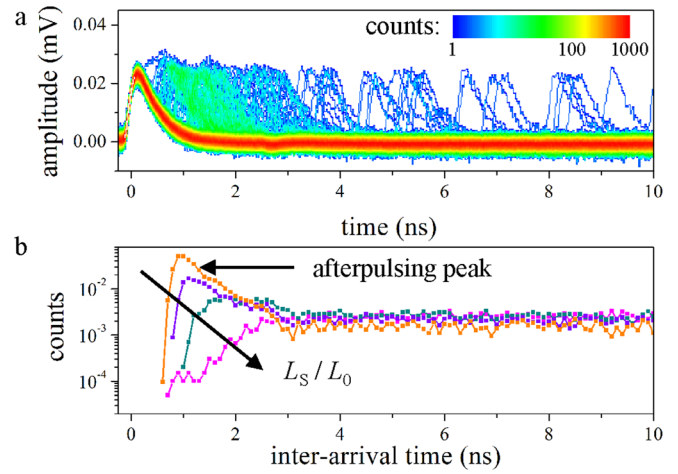


FIG. 3. (Color online) (a) Oscilloscope persistence map of the response of the 4-SNAP with $r = 1$ of Figures 2(a) and 2(b). The device was biased in the avalanche regime, at $I_B = 0.98 I_{SW}$. The persistence map represents the number of occurrences of a certain point (due to overlapping waveforms). (b) Histograms of the photoresponse pulse inter-arrival time for the same devices used in Figures 2(a) and 2(b). The devices were biased in the avalanche regime, at $I_B = 0.98 I_{SW}$.

recovery after an HSN event of the initiating section of a 3-SNAPs with the same series inductance as a correctly operating device, as shown in Figures 4(a) and 4(b), and as an afterpulsing device, as shown in Figures 4(c) and 4(d). For both devices, after the normal domain is formed, the nanowire switches back to the superconducting state when its critical current (I_C)¹⁵ becomes larger than the current through it (I_i). Once the superconductivity is restored, both I_i and I_C relax by increasing towards the steady-state values. While I_i increases with a time constant $(L_0/3 + L_S)/R_{load}$, I_C increases at the thermal relaxation rate, which decreases as the nanowire temperature (T) approaches the substrate temperature.^{5,16} Therefore, although the relaxation of I_C is initially faster than that of I_i , it slows down as T decreases. Figure 4(a) shows that, if the initial thermal relaxation rate is sufficiently shorter than the electrical relaxation rate, once the superconductivity is restored, both I_i and I_C increase towards the steady-state values without crossing again. Therefore, the device fully resets without afterpulsing, as shown in Figure 4(b). However, if the thermal and electrical relaxation rates are commensurate and the bias current is close to the steady-state critical current, I_i may exceed I_C again during the recovery, causing the relaxation-oscillation (RO) type behavior shown in Figure 4(c) (i.e., the afterpulsing repeats). The few-nanosecond-long RO phase in Figure 4(d) shows that our simulations could qualitatively reproduce the afterpulsing observed experimentally. We attributed the fact that the device relaxes to the superconducting state after the RO phase, instead of latching,¹⁷ to the slight imbalance between the current through the initiating and secondary sections (created as a result of the avalanche formation), which prevents all of the sections from latching to the normal state at the same time.

Although we did not observe afterpulsing on any devices with reset times longer than $\sim 1 \text{ ns}$, we observed afterpulsing on all of the devices with reset time below $\sim 1 \text{ ns}$. We were able to measure afterpulsing-free SNAPs with

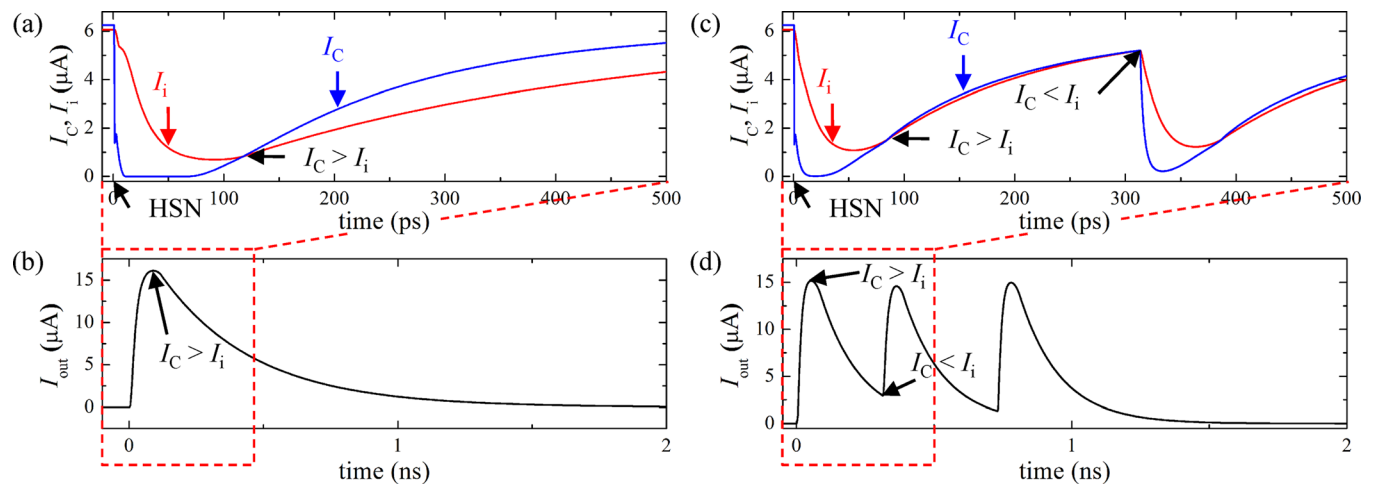


FIG. 4. (Color online) (a) Simulated recovery after a HSN event (at time 0 s, see arrow) of the current through the initiating section (I_i) of a 3-SNAP and its critical current (I_C). For the simulated device: $L_0 = 13$ nH; $L_S = L_0$ ($r = 0.5$). (b) Simulation of the output current (I_{out}) for the same device of Figure 4(a). The dashed frame encloses the region of the simulation shown in Figure 4(a). (c) Simulated recovery after an HSN event (at time 0 s, see arrow) of I_i and I_C for a 3-SNAP with $L_0 = 13$ nH; $L_S = 0.25 L_0$ ($r = 2$). (d) Simulated I_{out} for the same device of Figure 4(c). The first pulse starts at time 0 s, when the HSN event occurs in the initiating section. The second and third pulses start at time 310 ps and 730 ps, when I_i exceeds I_C during the current recovery as shown in Figure 4(c). The dashed frame encloses the initial stages of the simulation shown in Figure 4(c).

lower reset times than SNSPDs with the same area (up to a factor of ~ 2 by using 3-SNAPs with $r = 0.5$, see supplementary material¹⁸), indicating that SNAPs can in principle achieve lower reset time than SNSPDs with the same area. However, the speed of superconducting-nanowire-based detectors appears to be ultimately limited by the nanowire thermal-relaxation dynamics. Indeed, when the electrical- and thermal-relaxation time scales become comparable, superconducting-nanowire-based detectors appear to malfunction by either latching or afterpulsing, depending on the detector architecture and electrical environment.¹⁷

We investigated the speed limit of SNAPs by decreasing the L_S . As we decreased L_S , we observed that (1) SNAPs with low L_S ($r > 0.1$) emitted trains of current pulses when biased at a lower current than the onset of the arm-trigger regime; (2) the desired decrease in the detector reset time came at the price of an increase in the avalanche current, which decreased the bias range for the correct operation of the devices. Our results indicate that the reset time of SNAPs can be made lower than SNSPDs with the same area by decreasing L_S . However, the reset time could not be reduced below ~ 1 ns, as the devices showed afterpulsing. Based on our simulations, we attributed the unstable regime to the rebiasing of the SNAP after an HSN event occurred in one of the sections and the afterpulsing effect to the electrothermal relaxation of the device after an avalanche was triggered. We suspect that the limit on the reset time of ~ 1 ns we observed on our devices was due to the device materials and geometries we employed. Therefore, engineering the thermal environment of the superconducting nanowires (by modifying the substrate material or surface preparation or by patterning thermally conductive materials on the nanowires) may result in a decrease of the thermal-relaxation time, which is required to allow reducing the detector reset time below 1 ns.

The authors thank James Daley, Mark Mondol, and Professor Rajeev Ram for technical support. The work by F.

Marsili was supported by the Center for Excitonics, under Award No. DE-SC0001088. The work by F. Najafi was supported by IARPA. The work at MIT Lincoln Laboratory was sponsored by the United States Air Force under Air Force Contract No. FA8721-05-C-0002. Opinions, interpretations, recommendations, and conclusions are those of the authors and are not necessarily endorsed by the United States Government.

¹M. Ejmaes, R. Cristiano, O. Quaranta, S. Pagano, A. Gaggero, F. Mattioli, R. Leoni, B. Voronov, and G. Gol'tsman, *Appl. Phys. Lett.* **91**, 262509 (2007).

²F. Marsili, F. Najafi, E. Dauler, F. Bellei, X. Hu, M. Csete, R. J. Molnar, and K. K. Berggren, *Nano Lett.* **11**, 2048 (2011).

³G. N. Gol'tsman, O. Okunev, G. Chulkova, A. Lipatov, A. Semenov, K. Smirnov, B. Voronov, A. Dzardarov, C. Williams, and R. Sobolewski, *Appl. Phys. Lett.* **79**, 705 (2001).

⁴The factor ~ 4 increase in the SNR with respect to SNSPDs with the same wire width was achieved with 4-parallel-section SNAPs (4-SNAPs).

⁵F. Marsili, F. Najafi, C. Herder, and K. K. Berggren, *Appl. Phys. Lett.* **98**, 093507 (2011).

⁶For time scales of the order of 100 ps, the impedance of the series inductor was higher than R_{load} for all of the devices reported. Although neglecting R_{load} in the expression of r for the devices with the higher values of r and N was a more crude approximation, we could qualitatively predict the dependence of the avalanche current on N and r for all of the devices studied.

⁷ $r = 0.1, 0.12, 0.18, 0.25, 0.28, 0.5, 0.56, 1, \text{ and } 2$.

⁸In the unstable regime, the PCR could in principle be higher than the photon flux incident on the device.

⁹The spurious peak in the PCR vs I_B curves could be suppressed by increasing the trigger level of the discriminator of the pulse counter used for those measurements above the amplitude of the "small" pulses generated by the device (see supplementary material (Ref. 18)). We intentionally chose to count the pulses of both amplitudes to make the unstable regime evident on the PCR vs I_B curves.

¹⁰F. Najafi, F. Marsili, E. Dauler, A. J. Kerman, R. J. Molnar, and K. K. Berggren, "Timing performance of 30-nm-wide superconducting nanowire avalanche photodetectors" (unpublished).

¹¹F. Marsili, D. Bitauld, A. Gaggero, S. Jahanmirinejad, R. Leoni, F. Mattioli, and A. Fiore, *New J. Phys.* **11**, 045022 (2009).

¹²A. Divochiy, F. Marsili, D. Bitauld, A. Gaggero, R. Leoni, F. Mattioli, A. Korneev, V. Seleznev, N. Kaurova, O. Minaeva, G. Gol'tsman, K.

Lagoudakis, M. Benkhaoul, F. Lévy, and A. Fiore, *Nature Photon.* **2**, 302 (2008).

¹³In Figure 2(a), we intentionally chose photoresponse pulses without afterpulsing to highlight the apparent device speed-up with decreasing L_S .

¹⁴M. Fujiwara, A. Tanaka, S. Takahashi, K. Yoshino, Y. Nambu, A. Tajima, S. Miki, T. Yamashita, Z. Wang, A. Tomita, and M. Sasaki, *Opt. Express* **19**, 19562 (2011).

¹⁵As the critical current depends on the nanowire temperature, which is not homogeneous along the nanowire, we quote as the critical current the minimal value of the critical current spatial distribution (i.e., at the maximum of the temperature distribution).

¹⁶A. J. Annunziata, O. Quaranta, D. F. Santavicca, A. Casaburi, L. Frunzio, M. Ejrnaes, M. J. Rooks, R. Cristiano, S. Pagano, A. Frydman, and D. E. Prober, *J. Appl. Phys.* **108**, 084507 (2010).

¹⁷A. J. Kerman, J. K. W. Yang, R. J. Molnar, E. A. Dauler, and K. K. Berggren, *Phys. Rev. B* **79**, 100509 (2009).

¹⁸See supplementary material at <http://dx.doi.org/10.1063/1.3691944> for fabrication process and experimental setup; amplitude of the response pulses in the unstable regime; electrothermal simulation of 2- and 3-SNAPs in the unstable regime; dependency of the avalanche current on the number of sections and r ; discussion on the afterpulsing of sub-1-ns-reset-time devices; and Low-reset-time SNAPs.